AFTER 90 YEARS: CMOS-BASED HAFNIA-ZIRCONIA NANOMECHANICAL RESONATOR EXCEEDING AT-CUT QUARTZ TEMPERATURE STABILITY

*Troy Tharpe[1], Moumita Chakraborty[1], and Roozbeh Tabrizian[1]**

[1]Department of Electrical and Computer Engineering, University of Florida, Gainesville, FL 32611, USA

ABSTRACT

This paper reports on a temperature-stable hafnia-zirconia ($Hf_{0.5}Zr_{0.5}O_2$ or HZO) nanomechanical resonator with an overall frequency drift of 42 ppm over -40°C to 120°C. 90 years after the discovery of AT-cut quartz and its adoption for stable clock generation, the presented temperature-stable HZO resonator introduces a complementary metal oxide semiconductor (CMOS) based solution enabling monolithic integration of local and independent clocks in advanced processors for emerging artificial intelligence (AI) applications. The presented resonator operates in the first width-extensional (WE_1) mode at 65.6 MHz and is passivated with symmetric silicon dioxide (SiO_2) layers with thicknesses optimized for compensation of the first and second order temperature coefficients of frequency ($TCF_{1,2}$). For the first time, a third-order temperature characteristic is measured with two turn-over points at -12°C and 54°C. The frequency drift over -40°C to 120°C shows ~290 times reduction compared to an uncompensated HZO resonator with the same design, while offering a higher quality factor (Q) and fast pre-aging stress relaxation period. These unique characteristics, along with inherent CMOS-compatibility of the presented HZO-SiO_2 nanomechanical resonator paves the way for the realization of local clock arrays to serve in multi-core processors and emerging in-memory computing architectures built upon back-end-of-line (BEOL) ferroelectric hafnia devices.

KEYWORDS

Hafnia-zirconia, temperature stable, resonator, oscillator, on-chip clock, third order temperature characteristic.

INTRODUCTION

The need for efficient computing within large AI applications has introduced a new class of processors where CMOS-based devices (*e.g.*, ferroelectric random-access memories, ferroelectric tunnel junctions, Memristors) simultaneously serve as memory and logic, enabling substantial reduction of energy consumption and speed enhancement. In-memory computers require access to an array of local clocks to enable parallel processing essential for demanding AI applications. Conventional clock-generation paradigm, based on the use of an off-chip quartz crystal or Si MEMS oscillator, is not scalable to accommodate the growing needs of in-memory and multi-core computers. Relying on an external master clock substantially bottlenecks the efficiency and speed of computing by limiting parallel processing, inducing destructive electromagnetic field emissions, and imposing unnecessary timing and synchronization constraints. To address these challenges, there is an essential need for an on-chip temperature-stable nanoresonator technology with compatibility to advanced CMOS nodes and scalable size. Such technology enables the creation of spatially distributed and spread-spectrum clock arrays, allowing independent and parallel operation of numerous cores.

Previous demonstrations of CMOS-BEOL integrated clocks do not meet the needs of emerging AI and in-memory computing applications. First, their large size, compared to solid-state components, hinders their chip level arraying with these very large-scale integration (VLSI) components. Second, their temperature stability is significantly lower compared to quartz counterparts (*e.g.*, AT-cut quartz crystal oscillators (XOs)) used for clock generation.

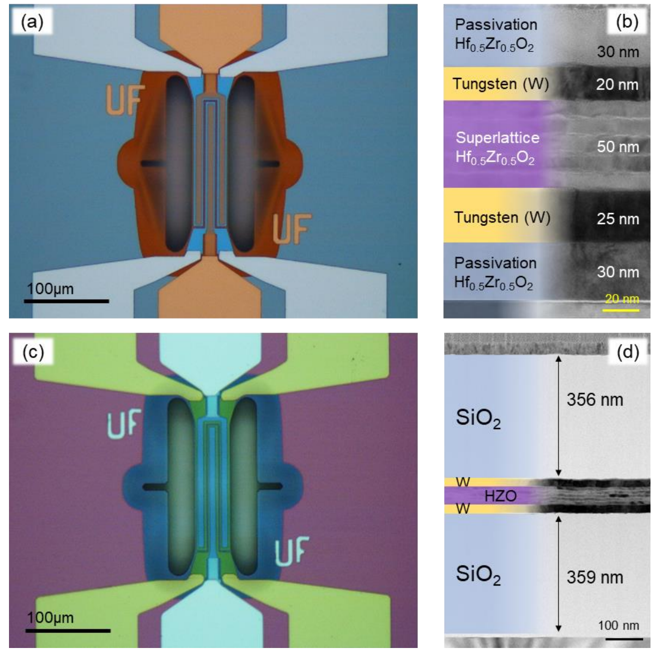

***Figure 1**: (a) Optical image of an uncompensated hafnia-zirconia nanomechanical resonator and (b) its cross-sectional TEM image highlighting constituent layers. (c) Optical image of a temperature-insensitive hafnia-zirconia resonator where symmetric SiO_2 layers are used for TCF_i compensation. (d) Cross sectional TEM image of a temperature insensitive HZO-SiO_2 resonator.*

An alternative technology leverages HZO nanomechanical resonators which show promise for CMOS integration within ferroelectric in-memory computers [1]. These HZO-based nanoresonators demonstrate high Qs [2], and exceptional conformality required for high density, three-dimensional spectral processing [3]. Despite their promise, uncompensated HZO nanomechanical resonators suffer from large temperature instability which hinders their application for stable clock generation. In this paper, we characterize this instability and realize temperature compensation of HZO nanomechanical resonators by symmetric layering with SiO_2 films to completely compensate first and second order temperature effects.

RESONATOR FABRICATION

To quantify the temperature coefficient of the young's modulus for HZO (TCE_{HZO}), investigate resonance frequency trends across temperature, and compensate temperature dependence, resonators both with and without SiO_2 compensation layers are fabricated. Uncompensated HZO resonators are realized from 50nm-thick, atomic layer deposited (ALD) HZO-alumina (Al_2O_3) superlattice transducers with ~20nm tungsten (W) electrodes, and 30nm HZO passivation layers according to previously published fabrication methods [1]. Figure 1 (a) depicts an optical image of an uncompensated, two-port, HZO resonator, designed to operate in width extensional (WE) modes with a width of 44 µm and length of 200 µm. Figure 1 (b) shows this device cross-section by transmission electron microscopy (TEM), with annotated layers.

To compensate HZO resonator's large negative temperature trend (discussed in the subsequent section) SiO_2 layers with a positive TCE_1 are incorporated into the resonant stack. These compensated HZO on SiO_2 resonators are fabricated by substituting top and bottom HZO passivation layers with plasma enhanced chemical vapor deposition (PECVD) SiO_2, deposited using a STS 310PC PECVD system. Compensated, temperature insensitive HZO resonators are fabricated using a reticle set and transducer thickness (20nm W/ 50nm superlattice HZO-Al_2O_3/ 25nm W) identical to uncompensated resonators to minimizing confounding variables. Figure 1 (c) depicts an optical image of a fabricated temperature insensitive, HZO-SiO_2 resonator. Figure 1 (d) shows a cross sectional TEM image for this device, highlighting symmetric SiO_2 layers with ~360nm thickness engineered for finite, i^{th} order *TCF* (TCF_i) compensation.

TEMPERATURE COMPENSATION

The TCF_i of any resonator is the i^{th} order rate of frequency change across temperature, normalized to the starting resonance frequency and temperature, given by:

$$TCF_i = \frac{1}{i!f_0|_{T=T_0}} * \frac{\partial^i f_T}{\partial T^i} \quad (1),$$

where f_0 is the resonance frequency at starting temperature T_0, f_T is the instantaneous resonance frequency, and T is the instantaneous temperature. The resonance frequency of the n^{th} order mode (f_n) for an isotropic, WE bulk acoustic wave (BAW) resonators is given by:

$$f_n = \frac{n}{2W} * \sqrt{\frac{E_{eq}}{\rho_{eq}}} \quad (2),$$

where W is the width of the resonator, E_{eq} is the equivalent Young's modulus of the composite resonator, and ρ_{eq} is the equivalent density of the composite resonator. Since density is agnostic to temperature change, applying Eq. 1 to Eq. 2 yields,

$$TCF_i = \frac{1}{2} * (TCE_{eq,i} + \alpha_{eq,i}) \quad (3).$$

Here, $TCE_{eq,i}$ is the i^{th} order temperature coefficient of the equivalent Young's modulus, and $\alpha_{eq,i}$ is the i^{th} order equivalent coefficient of thermal expansion. Extending Eq. 3 to a composite resonator with k layers yields [4],

$$TCF_i \approx \frac{1}{2} * \sum_k \frac{d_k}{d_{Res}} (TCE_{i,k} + \alpha_{i,k}) \quad (4),$$

where d_k is the thickness of the k^{th} layer within the composite resonator, and d_{Res} is the thickness of the entire resonator.

Compensation of resonator TCF_i requires the determination of each parameter within Eq. 4 and engineering of k^{th} layer thickness to achieve a net zero temperature characteristic. To achieve this, both ports of an uncompensated HZO resonator are pulsed poled into the negative polarization state (N state) and the forward transmission response (S_{21}) is measured at various temperatures using a Keysight N5222A vector network analyzer, heated chuck, and Instec mK2000 temperature controller. The uncompensated resonator is baked for 1 hour at 130ºC and the resonance frequency for the WE_1 mode is tracked from 59.94 MHz at 30°C to 58.02 MHz at 130°C, with magnitude S_{21} responses shown in Fig. 2 (a) and frequency shift depicted as stars within Fig. 2 (b). Each temperature point is held for 15 min to allow for temperature stabilization. Measured results are highly linear and an overall resonator temperature coefficient of frequency (TCF_{Res}) of -76.1 ppm/°C.

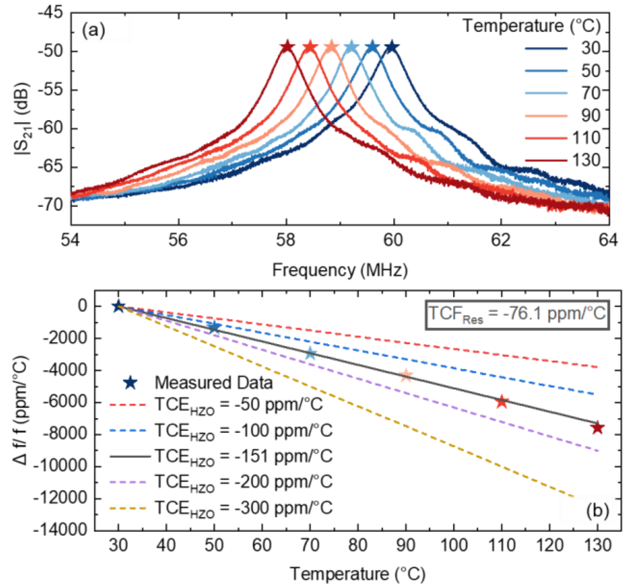

***Figure 2**: Experimental fitting of uncompensated HZO resonator TCF_{Res} and extraction of temperature coefficient of elasticity for hafnia-zirconia (TCE_{HZO}) via simulation: (a) Measured transmission response of uncompensated resonator over 30 °C to 130°C; (b) COMSOL simulated temperature characteristic is fitted to experimentally measured data to identify TCE_{HZO}.*

A COMSOL simulation of an uncompensated HZO resonator periodic slice is developed with thicknesses identified within Fig. 1 and material properties listed within Table 1. $TCE_{1,HZO}$ is then modified to match simulated temperature trends with measurements according to Eq. 4. Figure 2 (b) shows simulated resonance frequency temperature trends for varied values of 1^{st} order temperature coefficient of elasticity for hafnia-zirconia, with $TCE_{1,HZO}$ = -151 ppm/ºC exhibiting the closest fit to experimental TCF_{Res}.

***Table 1**: Material properties used for extraction of $TCE_{1,HZO}$ and determination of SiO_2 thickness (d_{SiO2}) for temperature compensation, via COMSOL simulation; ν: Poisson's ratio.*

Material Property	Value	Ref.
E_W	450 GPa	[5]
ν_W	0.26	[6]
$\alpha_{1,W}$	4.5 ppm/ºC	[7]
$TCE_{1,W}$	-137.3 ppm/ºC	[8]
E_{SiO2}	60 GPa	[9]
ν_{SiO2}	0.25	[9]
$\alpha_{1,SiO2}$	2.67 ppm/ºC	[9]
$TCE_{1,SiO2}$	163 ppm/ºC	[10]
$E_{HZO,Transducer}$	320 GPa	[11]
$E_{HZO,Passivation}$	285.43 GPa	[11]
ν_{HZO}	0.29	[12]
$\alpha_{1,HZO}$	4.5 ppm/ºC	[2]

This simulation is then extended to model a temperature compensated HZO resonator by including symmetric, top and bottom SiO_2 passivation layers with cross-section depicted in Fig. 3 (a) and properties presented in Table 1. SiO_2 thickness (d_{SiO2}) is varied, and resonance frequency simulated for the third width extensional mode (WE_3), shown in Fig. 3 (b), across 200°C of

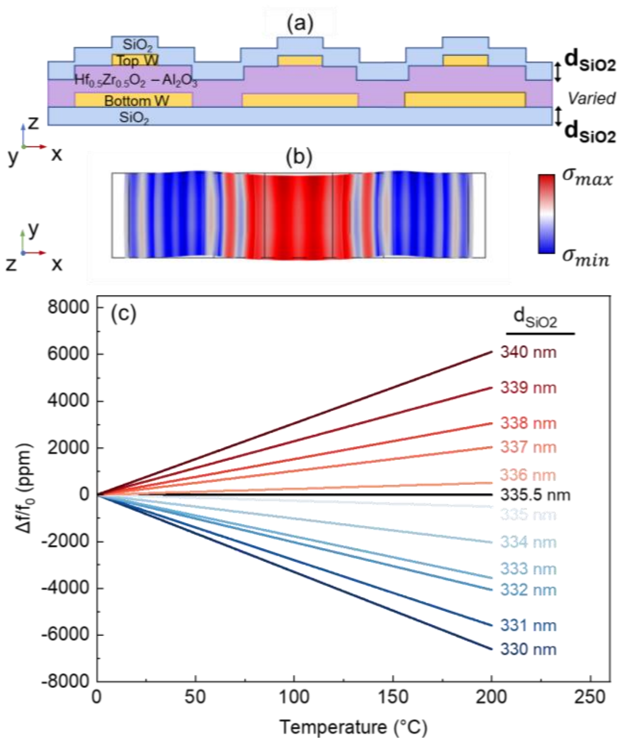

***Figure 3**: (a) Cross-sectional diagram of simulated temperature stable HZO-SiO_2 resonator. (b) Simulated WE_3 operational mode. (c) Resonance frequency change with temperature per varied SiO_2 thickness (d_{SiO2}) to identify d_{SiO2} needed for compensation of TCF_1.*

temperature change. Figure 3 (c) shows simulated resonance frequency variation with d_{SiO2} varied from 330nm to 340nm. A d_{SiO2} value of 335.5 nm minimizes Eq. 4 for a simulated $TCF_1 \approx 0$. For fabricated HZO-SiO_2 resonators, a larger d_{SiO2} of 360 nm is targeted to account for fabrication and simulation uncertainties.

RESONATOR RF CHARACTERIZATION

The room-temperature frequency responses of fabricated uncompensated HZO and temperature compensated HZO-SiO_2 resonators are characterized using a Radiant PiezoMEMS tester to wake-up and pole resonator ports to the N state [1], and Keysight N5222A to measure S_{21}. Figure 4 (a, b) depicts measured

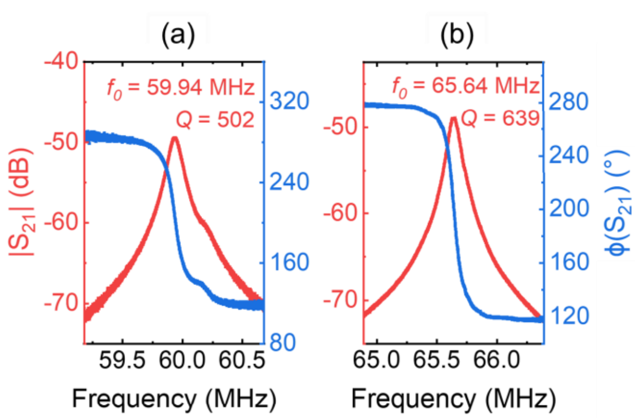

***Figure 4**: Measured transmission response magnitude ($|S_{21}|$) and phase ($\phi(S_{21})$) for (a) uncompensated and (b) temperature compensated HZO nanoresonators shown in Fig. 1, when operating in the first width-extensional mode.*

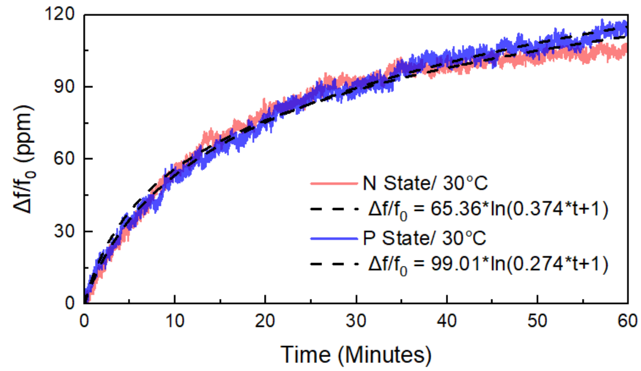

***Figure 5**: Stress-relaxation, pre-aging characteristic measured for two identical temperature-compensated HZO-SiO_2 resonators with transducers poled in opposite direction. Exceptional repeatability and natural logarithmic fit are evident.*

transmission response magnitude ($|S_{21}|$) and phase ($\phi(S_{21})$) for uncompensated HZO and compensated HZO-SiO_2 resonators operating in the WE_1 mode, respectively. Incorporation of ~360 nm compensation SiO_2 shifts the fundamental resonance from 59.94 MHz to 65.64 MHz and improves Q from 502 to 639.

OSCILLATOR TEMPERATURE STABILITY

To characterize frequency-temperature trends for HZO-SiO_2 resonators, compensated resonators are first subject to the same pre-measurement bake and pulsed poling procedure as uncompensated HZO resonators. Next, an oscillator is formed using a Zurich UHFLI 600 MHz Lock-in Amplifier to lock-in to the WE_1 mode of a 44 µm width and 200 µm length HZO-SiO_2 resonator (Fig. 1 (c)), with an input power of -15 dBm. Prior to TCF measurement, locked oscillations are sustained for 60 min at 30°C to mitigate stress

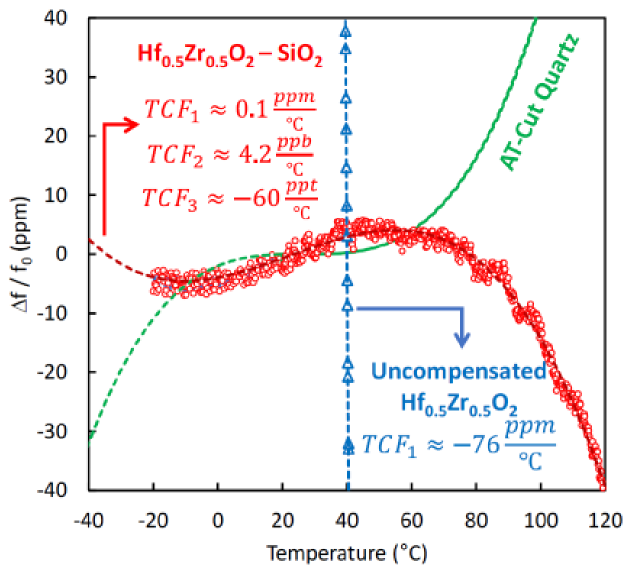

***Figure 6**: Comparison of the measured temperature characteristic of uncompensated and temperature-stable hafnia-zirconia resonators, highlighting ~290-times reduction in overall frequency drift across -40°C to 120°C. The performance is also compared with an AT-cut quartz oscillator [14]. 90 years after the discovery of AT-cut quartz, finally a CMOS-based nanoresonator technology exceeds its temperature stability, paving the way for on-chip clock generation in emerging advanced processors.*

relaxation effects on resonance frequency. Figure 5 depicts frequency change during this stress relaxation period for two identical, HZO-SiO_2 resonators, pulsed poled into opposing N and P polarization states. The close natural logarithmic fit and frequency drift agnostic to polarization direction matches initial aging trends in quartz XOs, and reveals initial frequency change to be primarily governed by stress relaxation [13].

Following 1 hour of stress relaxation, oscillators are again formed from uncompensated HZO and compensated HZO-SiO_2 resonators, using a lock-in amplifier, to measure the frequency drift across temperature sweeps over -20 °C to 120 °C. The results are compared in Fig. 6, along with the frequency-temperature trend of AT-cut quartz XOs [14]. The HZO-SiO_2 temperature-compensated oscillator shows ~290 times smaller frequency drift compared to its uncompensated HZO counterpart, allowing for the extraction of up to the third order TCF component. A TCF_1 = 0.1 ppm/°C, TCF_2 = 4.2 ppb/°C, and TCF_3 = -60 ppt/°C is extracted by polynomial fitting of measured frequency drift. Additionally, temperature compensated HZO-SiO_2 oscillators show ~50% lower frequency drift when compared to AT-cut quartz, highlighting their potential to replace non-integrated quartz clocks in emerging processors.

CONCLUSION

This paper reports for the first time, a CMOS compatible, HZO-SiO_2 based, temperature stable nanoresonator, with temperature stability exceeding that of AT-cut quartz, 90 years after its discovery [15][16]. To achieve this, uncompensated HZO resonators were fabricated, and temperature characteristic measured to extract a $TCE_{1,HZO}$ = -151 ppm/ºC, via simulation. Temperature compensated HZO-SiO_2 resonators were then realized with ~360 nm of top and bottom compensation SiO_2 to achieve near complete cancelation of TCF_1 and TCF_2 effects across -40 °C to 120 °C. A TCF_1 = 0.1 ppm/ºC, TCF_2 = 4.2 ppb/ºC, and TCF_3 = -60 ppt/ºC were extracted for HZO-SiO_2 oscillators by polynomial fitting of measured frequency drift. The presented temperature stable nanoresonators address the urgent need for on-chip, temperature-stable, clocks with compatibility to advanced CMOS nodes and scalable size. Such technology is poised to enable the creation of spatially distributed and spread-spectrum clock arrays for emerging, AI and in-memory computing applications.

ACKNOWLEDGEMENTS

This work is supported by the Defense Advanced Research Projects Agency through the Young Faculty Award (D19AP00044) and the National Science Foundation through the CAREER award (ECCS-1752206). The authors would also like to thank the University of Florida Nanoscale Research Facility staff for their great help regarding fabrication and material characterization throughout this project.

REFERENCES

[1] T. Tharpe, E. Hershkovitz, F. Hakim, H. Kim, and R. Tabrizian, "Nanoelectromechanical resonators for gigahertz frequency control based on hafnia–zirconia–alumina superlattices," *Nat. Electron.*, vol. 6, pp. 599–609, 2023, doi: 10.1038/s41928-023-00999-9.

[2] X. Q. Zheng, T. Tharpe, S. M. Enamul Hoque Yousuf, N. G. Rudawski, P. X. L. Feng, and R. Tabrizian, "High Quality Factors in Superlattice Ferroelectric $Hf_{0.5}Zr_{0.5}O_2$ Nanoelectromechanical Resonators," *ACS Appl. Mater. Interfaces*, vol. 14, no. 32, pp. 36807–36814, 2022, doi: 10.1021/acsami.2c08414.

[3] F. Hakim, N. G. Rudawski, T. Tharpe, and R. Tabrizian, "A ferroelectric-gate fin microwave acoustic spectral processor," *Nat. Electron.*, vol. 7, no. February, 2024, doi: 10.1038/s41928-023-01109-5.

[4] R. Tabrizian, G. Casinovi, and F. Ayazi, "Temperature-stable silicon oxide (SilOx) micromechanical resonators," *IEEE Trans. Electron Devices*, vol. 60, no. 8, pp. 2656–2663, 2013, doi: 10.1109/TED.2013.2270434.

[5] N. M. G. Parreira, N. J. M. Carvalho, and A. Cavaleiro, "Synthesis, structural and mechanical characterization of sputtered tungsten oxide coatings," *Thin Solid Films*, vol. 510, no. 1–2, pp. 191–196, 2006, doi: 10.1016/j.tsf.2005.12.299.

[6] P. O. Renault, K. F. Badawi, L. Bimbault, P. Goudeau, E. Elkaïm, and J. P. Lauriat, "Poisson's ratio measurement in tungsten thin films combining an x-ray diffractometer with in situ tensile tester," *Appl. Phys. Lett.*, vol. 73, no. 14, pp. 1952–1954, 1998, doi: 10.1063/1.122332.

[7] Y. Lee, Y. Goh, J. Hwang, D. Das, and S. Jeon, "The Influence of Top and Bottom Metal Electrodes on Ferroelectricity of Hafnia," *IEEE Trans. Electron Devices*, vol. 68, no. 2, pp. 523–528, 2021, doi: 10.1109/TED.2020.3046173.

[8] F. H. Featherston and J. R. Neighbours, "Elastic constants of tantalum, tungsten, and molybdenum," *Phys. Rev.*, vol. 130, no. 4, pp. 1324–1333, 1963, doi: 10.1103/PhysRev.130.1324.

[9] G. Carlotti, L. Doucet, and M. Dupeux, "Comparative study of the elastic properties of silicate glass films grown by plasma enhanced chemical vapor deposition," *J. Vac. Sci. Technol. B Microelectron. Nanom. Struct.*, vol. 14, no. 6, pp. 3460–3464, 1996, doi: 10.1116/1.588780.

[10] R. Melamud *et al.*, "Temperature-Insensitive Composite Micromechanical Resonators," *J. Microelectromechanical Syst.*, vol. 18, no. 6, pp. 1409–1419, 2009, doi: 10.1109/JMEMS.2009.2030074.

[11] T. Tharpe, X. Zheng, P. X. Feng, and R. Tabrizian, "Resolving Mechanical Properties and Morphology Evolution of Free-Standing Ferroelectric Hf0.5Zr0.5O2," *Adv. Eng. Mater.*, vol. 2101221, pp. 1–9, 2021, doi: 10.1002/adem.202101221.

[12] S. S. Fields *et al.*, "Compositional and phase dependence of elastic modulus of crystalline and amorphous Hf 1- x Zr x O 2 thin films Compositional and phase dependence of elastic modulus of crystalline and amorphous Hf 1- x Zr x O 2 thin films," *Appl. Phys. Lett.*, vol. 102901, no. February, 2021, doi: 10.1063/5.0044702.

[13] J. R. Vig and T. R. Meeker, "The aging of bulk acoustic wave resonators, filters and oscillators," *Proc. Annu. Freq. Control Symp.*, pp. 77–101, 1991, doi: 10.1109/freq.1991.145888.

[14] J. A. Kusters and J. R. Vig, "Hysteresis in Quartz Resonators—A Review," *IEEE Trans. Ultrason. Ferroelectr. Freq. Control*, vol. 38, no. 3, pp. 281–290, 1991, doi: 10.1109/58.79613.

[15] F. R. Lack, G. W. Willard, and I. E. Fair, "Some improvements in quartz crystal circuit elements.," *Bell Syst. Tech. J.*, vol. 13, no. 3, pp. 453–463, 1934.

[16] I. Koga, "Thermal Characteristics of Piezo-Electric Oscillating Quartz Plates," *Rep. Radio Res. Japan*, vol. 4, no. 2, 1934.

CONTACT

*Troy Tharpe, tel: +1-321-432-9557; ttharpe@ufl.edu.
*Roozbeh Tabrizian, tel: +1-352-846-3017; rtabrizian@ece.ufl.edu.